Connections between magnetic correlations and local crystalline structure in two dilute magnetic semiconductors: Li(Zn,Mn)As and (Ba,K)$(Zn,Mn)_2As_2$

Nicolas Andrew Ducharme

A capstone report submitted to the faculty of

Brigham Young University

In partial fulfillment of the requirements for the degree of

Bachelor of Science

Benjamin Frandsen, Advisor

Department of Physics and Astronomy

Brigham Young University

April 23, 2020

ABSTRACT

Connections between magnetic correlations and local crystalline structure in two dilute magnetic semiconductors

Nicolas Andrew Ducharme

Department of Physics and Astronomy

Bachelor of Science

Dilute magnetic semiconductors (DMSs) are of interest to physicists and materials scientists due to their potential applications in spintronics and quantum computing. The research I will present is not directly aimed at spintronic or quantum computing applications. Rather, it is aimed at understanding the detailed atomic and magnetic structure of DMSs, which will enable a more fundamental understanding of their properties and facilitate future applications. Two DMSs, Li(Zn,Mn)As and (Ba,K)$(Zn,Mn)_2As_2$ were investigated experimentally, with the data analyzed via pair distribution function (PDF) analysis of x-ray and neutron scattering data. Li(Zn,Mn)As was found to lack local structural deviations and possesses only weak magnetic order, while (Ba,K)$(Zn,Mn)_2As_2$ was found to have significant local structural deviations and possess more robust magnetic order. These findings suggest that useful magnetic correlations may be connected to local structural deviations.

Keywords: dilute magnetic semiconductor; local structure; magnetic correlations; short-range magnetic order; spintronics

Acknowledgments

Before all else, I'd like to thank my family for always encouraging me in whatever I choose to do and for fostering my curiosity.

I'd also like to thank Dr. Frandsen, who allowed me to ask and re-ask many questions related to this project. I also thank Dr. Frandsen for the effort he puts in to making his research group fun to work in and the sense of community I've felt there.

Lastly, I'd like to thank the Department of Physics and Astronomy at Brigham Young University for the opportunity to gain experience in research while also being paid.

Table of Contents

List of Figures

List of Tables

Chapter 1 Introduction

In this chapter, I will briefly address the topics of electronic semiconductors, magnetism, and magnetic semiconductors in preparation for later discussion on the topic of my research: the atomic and magnetic characteristics of $Li(Zn,Mn)As_2$ and $(Ba,K)(Zn,Mn)_2As_2$.

1.1 Electronic semiconductors

Electronic semiconductors are found in nearly all the electronic devices we use daily. These materials exhibit great versatility, with behavior ranging from that of an insulator to that of a metal. Physicists and materials scientists have spent innumerable hours in researching traditional electronic semiconductors, which has led to numerous technological breakthroughs beyond electronic applications. Khetani and Bhatia [1] discuss how semiconductor-driven microtechnology has allowed for the fabrication of microscale tissue subunits. Hoffman *et al.* [2], in citing numerous sources, discuss the application of semiconductors to photocatalysis in order to destroy bacteria and viruses, inactivate cancer cells, control odors, produce hydrogen gas, aid in the fixation of nitrogen, and clean up oil spills. My research is not related to any of these electronic or biological applications; I only mention them here to demonstrate that electronic semiconductors have many wide-ranging applications.

Most modern semiconductor devices are created by introducing non-semiconductor chemical elements—commonly referred to as 'impurities'—into the semiconductor's crystalline lattice. By introducing these elements—also known as 'doping' the semiconductor—the behavior of the device is modified, particularly the electrical conductivity. Later, I will discuss magnetic semiconductors and the role played by magnetic impurities, as magnetic semiconductors were the subject of the research I will present.

1.2 Magnetism

In preparation for a discussion on magnetic semiconductors, in this section I will convey a basic conceptual explanation of magnetism. Magnetic fields can originate from both the magnetic moment of particles and the movement of charged particles. In this section, I will focus only on magnetism resulting from magnetic moments, as my research deals only with that type of magnetism. This type of magnetism is intrinsically a quantum mechanical phenomenon that arises from the 'spin' of particles. This unfortunate name can be confusing as the particles are not spinning, yet they nevertheless possess intrinsic angular momentum as if they were spinning. This angular momentum imbues particles with an intrinsic magnetic dipole moment which serves as the origin of magnetism in materials. All electrons have a spin of magnitude ½, though the direction in which this spin vector points can vary. Figures depicting particle spin, such as Figure 1.1, often indicate a direction of rotation which, by the right-hand rule, indicates the direction of the spin vector: up or down. Said figures are merely used to aid visualization and should not be taken as literal representations of what the electron is doing.

Electrons are always either in a spin-up state, or a spin-down state. The magnetic contribution of a spin-up state cancels that of a spin-down state. As a result, magnetic atoms are

only those which have unpaired spins, i.e., more spin-up electrons than spin-down electrons, or vice versa. However, even if an atom has a net magnetic moment, a collection of magnetic atoms often is *not* magnetic. This lack of magnetism is a result of the net magnetic moment of one atom cancelling that of another atom.

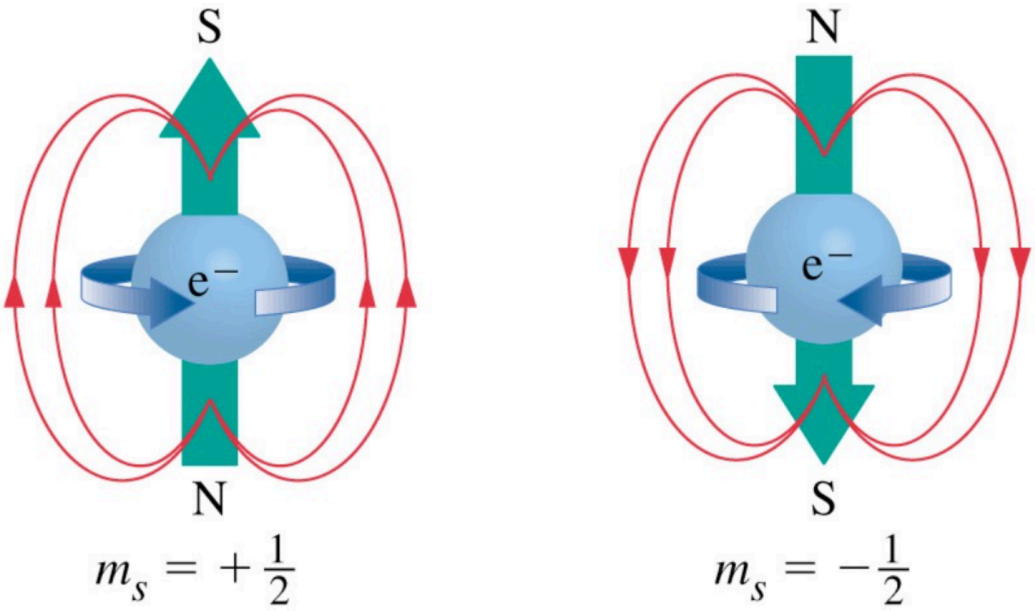

Figure 1.1 Magnetic spin moments. A spin-up electron (left) and a spin-down electron (right). Both the spin-up and spin-down electrons have a spin magnitude of 1/2, as the spin magnitude is a fundamental property of the electron. The magnetic field lines (red) produced by each electron's spin are also shown. Image from https://i.stack.imgur.com/qigFz.png in January 2020.

Ferromagnetism refers to the situation in which the magnetic moments of neighboring atoms are aligned with each other. A grouping of ferromagnetically aligned atoms resulting in a net magnetic moment is referred to as a 'magnetic domain' and is illustrated in Figure 1.2. When a material's magnetic domains align, the material has macroscopic magnetic behavior. The more domains that are aligned, the greater the net magnetic moment and, by extension, the greater the strength of the overall magnetism. When ferromagnets are raised above their Curie temperature—also referred to as their transition or ordering temperature—thermal fluctuations

prevent the magnetic moments from aligning in a static configuration. This results in the material becoming paramagnetic until it is lowered below its Curie temperature.

When magnetic materials are placed in an external magnetic field, the magnetic domains align with—or sometimes against—the field. Materials whose domains initially align with the field but later relax to a disordered state in its absence are called paramagnetic. By contrast, the magnetic domains in a ferromagnet remain aligned in the direction in which the field was applied even after removal of the field.

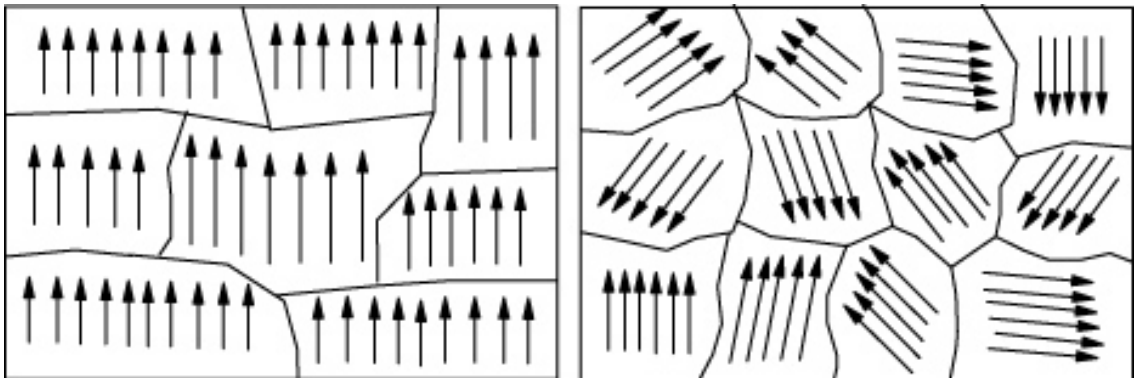

Figure 1.2 Each arrow represents the orientation of an atomic spin. Cells, or groups, of arrows represent magnetic domains. The magnetic domains of a magnetized material (left) and an unmagnetized material (right) are shown. Image from J A Souza and R F Jardim, "Electrical transport in disordered and ordered magnetic domains under pressures and magnetic fields," J. Phys. D 42, 3 (2009).

Ferromagnets display magnetic hysteresis, meaning they 'remember' the external magnetic fields they have experienced. In more technical terms, once the domains are aligned with an external field, there exists a minimum field strength (the coercive field) that must be applied in the opposite direction to reverse the direction of the net magnetization of the domains. Magnetic hysteresis has proven useful in digital memory since 1953 when the first hard drives were invented [3].

1.3 Magnetic semiconductors

In this section I will discuss some important characteristics of magnetic semiconductors. Further information can be found in the comprehensive review by Dietl and Ohno [4]. Magnetic semiconductors exhibit ferromagnetism, or some other type of magnetic order, in addition to their electronic properties. Some such semiconductors are intrinsically magnetic, while others become magnetic only after doping with magnetic atoms. Doping with magnetic atoms introduces unpaired spins, thereby allowing the possibility of establishing ferromagnetic order in the material. For example, manganese is often used as a magnetic dopant, since the Mn^{2+} ion contains five unpaired spins ($S = 5/2$). The dopant atoms are usually present in small concentrations (15% or less of the total number of atoms), in which case the materials are often referred to as "dilute magnetic semiconductors". Since these dilute magnetic semiconductors offer greater tunability of both the electronic and magnetic properties than is offered by intrinsically magnetic semiconductors, most potential technological applications focus on doped magnetic semiconductors.

The type of dopant and doping concentration influence both the electronic and the ferromagnetic properties of the material. In some cases, a single type of dopant atom introduces both spins and mobile carriers into the system, meaning that the magnetic and electronic properties cannot be modified independently. However, by selecting two different types of dopants, one that provides mobile charge carriers without spins and the other that provides spins without mobile charge carriers, the material's electronic properties can be manipulated independently of its magnetic properties. This thesis will focus on this latter type of doped magnetic semiconductor. Finally, I note that to be of practical use, dilute magnetic

semiconductors must have a Curie temperature at, or preferably above, room temperature. All currently known dilute ferromagnetic semiconductors have Curie temperatures below room temperature, but progress is gradually being made to raise the Curie temperature by engineering known materials or discovering new materials.

1.4 Motivation

In comparison to materials where the electronic and magnetic properties cannot be tuned separately, dilute magnetic semiconductors have greater applicational versatility. For this reason, understanding the fundamentals behind dilute magnetic semiconductors has the potential to transform technology as electronic semiconductors already have (see Section 1.1).

This technological transformation may come about through applications to spintronics, which refers to devices that utilize both the charge and spin of electrons to achieve novel functionalities. Dietl and Ohno [4] described how hole-mediated ferromagnetism in dilute magnetic semiconductors allows for easy magnetization manipulation and switching by doping, codoping, strain, electric field, and light, highlighting the versatility of these materials in spintronic applications. Li *et al.* [5] also described applications of dilute magnetic semiconductors to spintronics, as well as applications to quantum computing, by independently manipulating the spin and charge of electrons.

The research I will describe is not intended to be directly applied to spintronics or quantum computing; rather, its purpose is to develop a better understanding of the fundamental physical properties of dilute magnetic semiconductors. Developing this understanding will make future applications possible.

1.5 Previous work on Li(Zn,Mn)As and (Ba,K)(Zn,Mn)$_2$Li$_2$

The research I present focuses primarily on the atomic and magnetic structures of Li(Zn,Mn)As and (Ba,K)(Zn,Mn)$_2$Li$_2$. Below are summarized published findings on these compounds.

Deng *et al.* [6] described the crystallographic structure and ferromagnetic properties of Li(Zn,Mn)As and suggested that said properties may be attributed to excess lithium in substitutional zinc sites providing holes as mobile charge carriers and dilute amounts of manganese providing spins. However, Deng's treatment of Li(Zn,Mn)As was primarily focused on the compound's synthesis and observations of its properties rather than on investigating why it has those properties.

Zhao *et al.* [7] first reported the synthesis of the dilute magnetic semiconductor (Ba,K)(Zn,Mn)$_2$As$_2$, in which potassium provides holes and manganese provides spins. This material has a relatively high Curie temperature of 180 K. Frandsen *et al.* [8] studied the crystallographic and magnetic structures of (Ba,K)(Zn,Mn)$_2$As$_2$ through atomic and magnetic pair distribution function analysis, noting a change in curvature of the temperature-dependent unit cell volume of the average tetragonal crystallographic structure at the ferromagnetic ordering temperature. In this same paper Frandsen *et al.* also noted a local structural deviation from the average crystallographic structure and robust ferromagnetic correlations.

1.6 Scientific question addressed by this research

This research builds upon existing analysis of Li(Zn,Mn)As and (Ba,K)(Zn,Mn)$_2$As$_2$ with the express intent of probing the connections, or lack thereof, between local structure and

magnetic correlations. The existing literature on these compounds suggests that there *may* be some connection between local structural deviations and magnetic correlations, though the investigation of this connection itself has not been the primary focus of much research (see section 1.5).

1.7 Summary of results

Li(Zn,Mn)As was found to exhibit no significant local structural deviation from the global structure. Furthermore, it was found to lack any observable magnetic correlations in the pair distribution function data, indicating that the ferromagnetism is very weak.

$(Ba,K)(Zn,Mn)_2As_2$ was found to have local structural deviations from the average structure, in agreement with Frandsen *et al.* [8] Additionally, it was found to have observable ferromagnetic correlations in the data, indicating more robust ferromagnetism.

1.8 Overview

To demonstrate the conclusions stated in Section 1.7, in Chapter 2 I will discuss the methods used to analyze the data. I will not discuss the methods used to collect these data discussed in detail, as I did not participate in their collection. In Chapter 3, I will describe the analysis performed using the methods of Chapter 2 and will discuss the conclusions my advisor and I reached.

Chapter 2 Methods

The primary goal of this chapter is to familiarize you with the experimental techniques and software tools that were used for data analysis on this project. Additionally, this chapter is aimed at assisting future students with getting started on similar data analysis projects. For these purposes, I will discuss the pair distribution function, the PDFgui program, and the diffPy.mpdf software package.

2.1 Pair Distribution Function (PDF)

Pair distribution functions (PDFs) have been used to understand material structures since as early as 1935 [9] Recently, researchers including Proffen [10], Frandsen [8], Zheng [11], and others have employed PDF analysis to probe the details of many materials. For an in-depth derivation of the PDF, you may refer to the work of Egami and Billinge [12].

2.1.1 Atomic PDF

The analytical expression for the atomic PDF $G(r)$ for an arbitrary collection of atoms in a material is

$$G(r) = \frac{1}{r}\sum_{i \neq j} \frac{b_i b_j}{\langle b \rangle^2} \delta(r - r_{ij}) - 4\pi r \rho_0, \quad (1)$$

where the double sum runs over all the atoms in the material, b_i and b_j are the scattering lengths of the i^{th} and j^{th} atoms, $\langle b \rangle$ is the average scattering length of the entire material, r is the distance in real space, r_{ij} is the distance between atoms i and j, and ρ_0 is the average number density of atoms. Conceptually, the pair distribution function is related to the probability of finding two atoms separated by a specified distance within a material [13]. In this sense, it provides a map of inter-atomic correlations on an angstrom length scale. A simple schematic of this is shown in Figure 2.1. This information allows the researcher to characterize a material's unit cell, as well as account for its thermal fluctuations, Coulomb interactions, and other important properties [10].

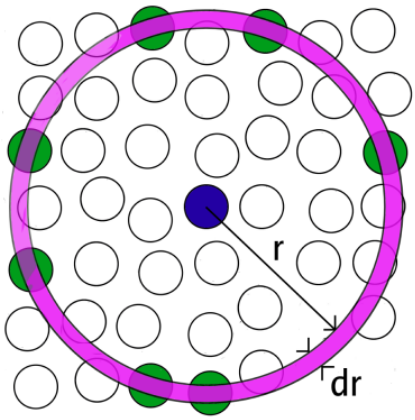

Figure 2.1 A one-dimensional example of what the pair distribution function does. The PDF would determine the probability that particles would be found within the range *dr* at a distance *r* from the blue particle. In this case, there are seven particles (green) that fall within this range at the shown distance. Image from http://isaacs.sourceforge.net/phys/rdfs.html in February 2020.

Experimentally, $G(r)$ is obtained as the inverse Fourier transform of the x-ray or neutron scattering pattern, as given by

$$G(r) = \frac{2}{\pi}\int_0^\infty Q(S(Q) - 1)\sin Qr \ \mathrm{d}Q,$$

where $\hbar Q$ is the magnitude of the momentum transfer vector of the scattered x-ray or neutron (hence Q has units of inverse length), $S(Q)$ is the normalized and dimensionless scattering intensity, and r is distance in real space. The analytical expression for $G(r)$ given previously can be computed for a structural model and compared to the experimentally obtained PDF, allowing for refinement of the structural model until it provides the best fit to the data. Notably, the inverse Fourier transform includes both Bragg peaks that encode information about the long-range, average structure as well as diffuse scattering, which contains information about short-range, local correlations that deviate from the average structure [10,14]. The location of peaks in the inverse Fourier transform indicates the distances by which atoms are likely to be separated. The higher and sharper the peak, the more likely that atoms are separated by that distance. Due to its sensitivity to the local structure, PDF analysis was selected as the primary method of analysis for the research I conducted. Specifically, analysis was performed on data collected from x-ray scattering experiments at Brookhaven National Laboratory and neutron scattering experiments performed at Oak Ridge National Laboratory. I did not participate in these experiments.

PDF analysis can be applied to deduce the separation distance of atoms in a crystalline lattice. The lattice vector magnitudes *a*, *b*, and *c* can be determined along with the angles between them α, β, and γ. Figure 2.2 shows these six parameters. Crystal families are composed of lattices that have similar parameters. For example, lattices with $a = b = c$ and $\alpha = \beta = \gamma = 90°$

are called cubic, while ones with $a = b \neq c$ and $\alpha = \beta = \gamma = 90°$ are called tetragonal. Both $Li(Zn,Mn)As_2$ and $(Ba,K)(Zn,Mn)_2As_2$ have crystal structures and unit cells much more complicated than that shown in Figure 2.2, as their unit cells contain multiple elements, whereas Figure 2.2 shows a unit cell with all atoms of the same element. I only include this figure as an introduction to the unit cell and it should not be taken as a representation of the actual crystal structures of the materials I researched.

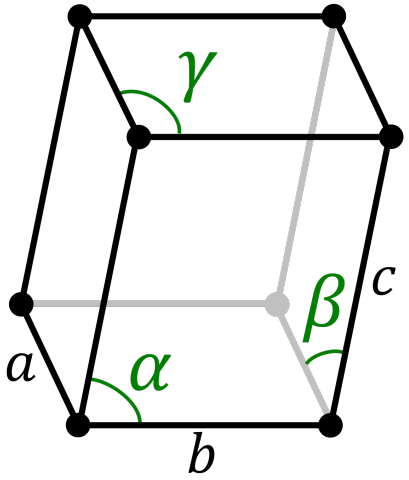

Figure 2.2 An arbitrary triclinic unit cell. The black dots at each corner represent the positions of atoms. The lattice vectors have lengths a, b, and c while the angles between them are α, β, and γ. Image from https://en.wikipedia.org/wiki/Triclinic_crystal_system in February 2020.

Peaks in the PDF pattern occur at distances by which two atoms are likely to be separated. Atomic PDF analysis also allows for analysis of short-range motional correlations. Even in a perfect crystal, these peaks will not be infinitely sharp, because vibrations result in a distribution of instantaneous positions around some average position. These deviations are described by the atomic displacement parameters (ADPs). PDF peaks at short interatomic spacings tend to be narrower than those at longer distances, because the vibrational motions of two nearby atoms are more likely to be correlated with each other than the motions of two widely separated atoms. Hereafter, these short-range motional correlations proportional to 1/r

will be referred to as δ_1, while those proportional to $1/r^2$ will be referred to as δ_2. The parameters δ_1 and δ_2 contribute to the peak width as shown mathematically in Eq. (2) [15], where σ_{ij} is the overall width of the peak corresponding to the distance r_{ij} between atoms i and j, σ'_{ij} is the peak width taking into account only the ADPs, and Q_{broad} is a property of the instrument used to collect the data that leads to peak broadening. According to Eq. (2), higher values of δ_1 and δ_2 lead to sharper peaks, which indicates stronger short-range correlations in atomic motion.

$$\sigma_{ij} = \sigma'_{ij}\sqrt{1 - \frac{\delta_1}{r_{ij}} - \frac{\delta_2}{r_{ij}^2} + Q_{broad}^2 r_{ij}^2} \tag{2}$$

2.1.2 Magnetic PDF (mPDF)

PDF analysis of neutron scattering data can also be used to determine the spatial separation and relative orientation of magnetic moments (referred to as magnetic correlations) [16]. Such analysis is known as magnetic PDF (mPDF) analysis. This analysis requires that the data encode information related to the magnetic moments and, ideally, ignore other effects. Neutrons, being electrically neutral, are unaffected by Coulombic interactions, yet they still have an intrinsic magnetic moment [17]. Therefore, neutrons are good candidates for capturing data related to magnetic moments. As a result, I performed all mPDF analysis on neutron scattering data.

The mPDF $d(r)$ from a collection of spin-only magnetic moments is given by

$$d(r) = \left(\frac{3}{N_s 2S(S+1)} \sum_{i \neq j} \left[\frac{A_{ij}}{r} \delta(r - r_{ij}) + B_{ij} \frac{r}{r_{ij}^3} \Theta(r_{ij} - r) \right] - \frac{2}{3} \langle m \rangle r \right) * \mathcal{M} + d_{para}, \quad (3)$$

where N_s is the number of moments, S is the spin quantum number, r_{ij} is the distance between moments i and j, A_{ij} and B_{ij} encode the spin-spin correlations transverse and parallel to the vector $\mathbf{r}_{ij}$, $\langle m \rangle$ is the net magnetization density, * is the convolution operator, $\mathcal{M}$ is the real-space spin density distribution of the individual magnetic moments, and d_{para} is the contribution from individual moments that is independent of any spin-spin correlations and results only in a peak at very low r, below the nearest-neighbor spin separation distance. Further details can be found in [18]. Experimentally, the mPDF is simply the inverse Fourier transform of the intensity of neutrons scattered from the magnetic moments in the material rather than the nuclei. Standard PDF experiments conducted at neutron sources, such as the experiments that yielded the data being analyzed in this work, result in a combined atomic and magnetic PDF signal $G(r) + d(r)$. Due to differences in the scattering strength of nuclei compared to magnetic moments, the mPDF $d(r)$ is often one to two orders of magnitude smaller than the atomic PDF $G(r)$.

One important factor in mPDF analysis is the magnetic propagation vector. The magnetic propagation vector describes the fraction of a complete cycle by which magnetic moments differ under translation by one unit cell. For ferromagnets, the magnetic propagation vector is (0, 0, 0), which indicates that in the x-, y-, and z-directions, the magnetic moment orientation differs by zero cycles (i.e., the orientation is identical) from moment to moment. Antiferromagnets have nonzero propagation vectors.

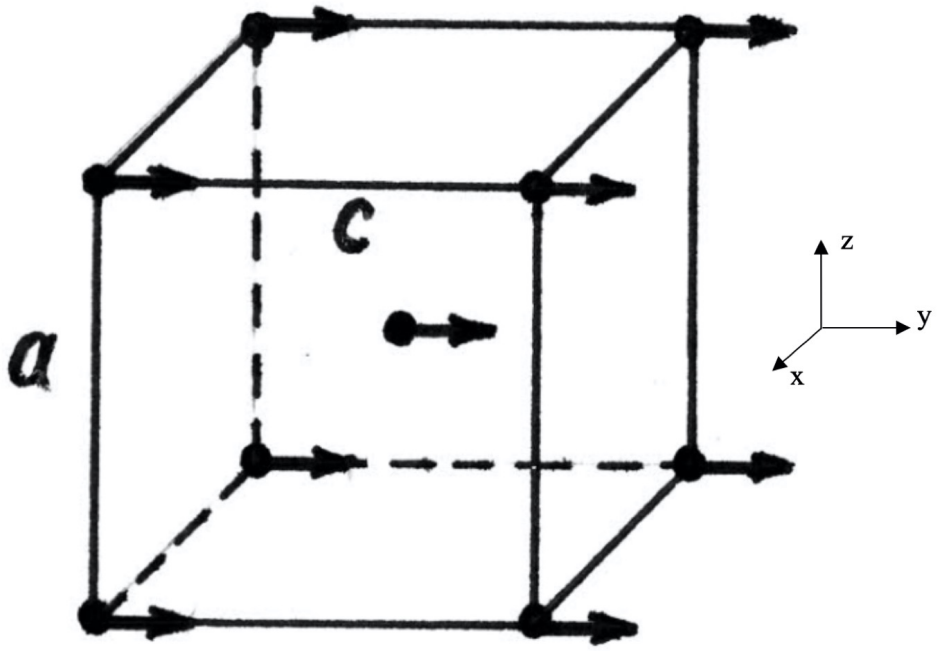

Figure 2.3 Body-centered cubic unit cell for a ferromagnetic material. Magnetic moment locations are represented by black dots. Magnetic moment vectors are shown as arrows. All symmetrically equivalent magnetic moments are oriented in the same direction, namely the (0, 1, 0) direction. This indicates that in the x-, y-, and z-directions the magnetic moments change by zero cycles form moment to moment. Image from Y. Mnyukh, American Journal of Condensed Matter Physics **4**, (2014).

The magnetic basis vectors indicate the magnitude and orientation of the material's magnetic moments. Typically, the magnetic basis vectors are unknown and are therefore refinement parameters in mPDF analysis. Figure 2.3 shows a unit cell whose magnetic basis vectors would be (0, 1, 0), with an arbitrary magnitude.

In a typical mPDF refinement, the ordered scale factor is one of the free parameters. This scale factor describes how strongly the magnetic moments maintain a definite orientation relative to one another. The larger the ordered scale factor, the more correlated magnetic moments are.

Another related refinement parameter is the damping factor. The damping factor describes how much the magnetic signal strength decreases with distance due to a finite

correlation length. In the limit of infinitely long-range magnetic correlations, the damping factor is zero, and the mPDF remains undamped even over very long distances.

2.2 PDF Graphic User Interface (PDFgui)

The pair distribution function graphic user interface (PDFgui) program [15] was developed to allow for easy calculation of the atomic PDF and refinement of structural models against experimental PDF data. PDFgui uses the refinement parameters described in section 2.1.1 to perform a least-squares fit to the PDF to experimental data. An example of a PDF fit is shown in Figure 2.4.

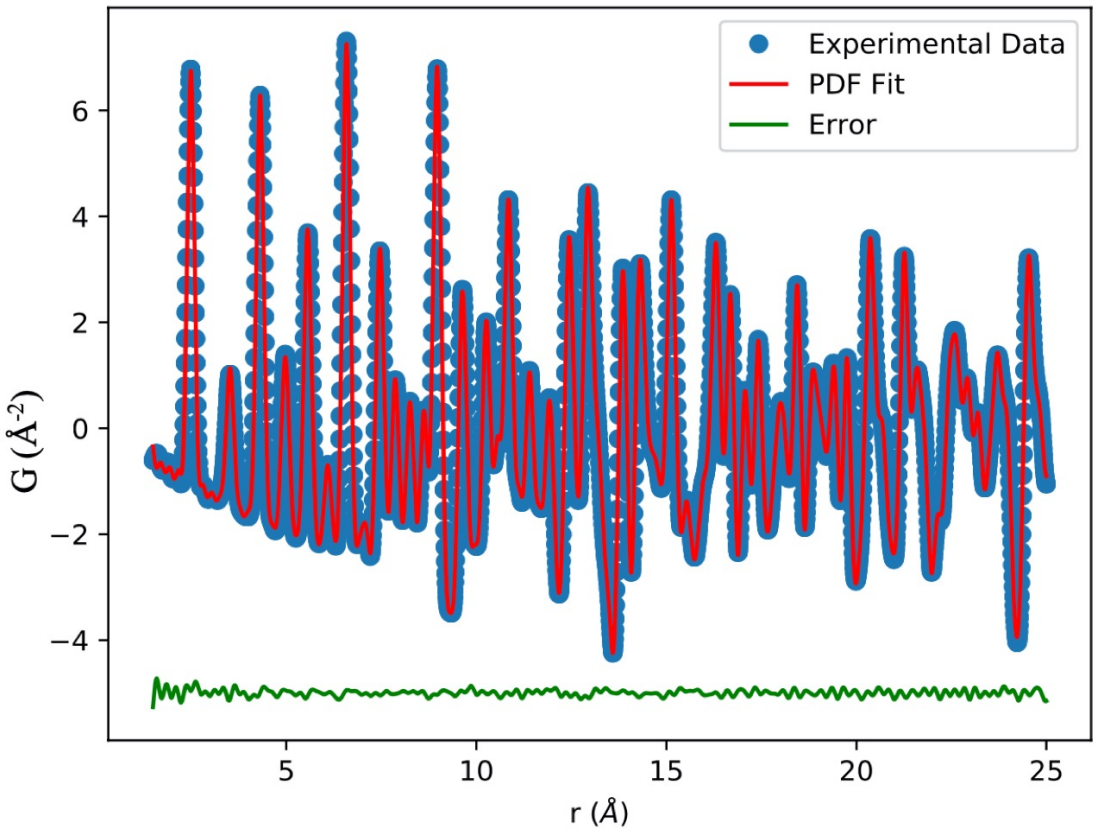

Figure 2.4 Example of a PDF fit to x-ray diffraction data for nickel. The error between the fit and experimental data has been offset by -5 for clarity.

Although relatively easy to use, there are a few details that I find important to keep in mind in order to achieve high-quality fits with the PDFgui. These details include the order of parameter refinement and knowing when fitting parameters are unphysical, as well as a few general tips.

2.2.1 General tips

When beginning a new fit, on the 'Data Set Configuration' pane it is important to enter the correct values of 'Qdamp' and 'Qbroad'. These values are unique to the instrument that was used to collect the data and will usually be provided by whoever recorded the data.

It is also important to limit the 'Fit Range.' Fitting over large ranges takes a very long time, and often does not yield any useful information beyond that from shorter ranges.

After each refinement, painting over the refined parameter values on the 'Parameters' pane and selecting 'Copy refined to initial' allows for additional refinement, using the refined values of the previous run as a starting point.

The quantitative quality of each fit is described by the 'rw' value listed on the 'Results' pane. This value is essentially the percent error of the fit, so the lower it is, the better. In order to improve this value, see the tips listed in sections 2.2.2 and 2.2.3.

2.2.2 Order of parameter refinement

Refining parameters in a non-ideal order often leads to non-physical values and/or low-quality fits. This section will provide generalized advice on how the parameters described in section 2.1.1 should be handled.

The more parameters that are free for refinement, the slower the refinement, so it is generally best to only refine one to three parameters at a time. Once these parameters have been refined and rerunning the fits no longer yields a significantly lower error, fix the refined parameters.

Following this procedure, the following order will ordinarily yield high-quality fits: lattice vector magnitudes and scale factor, lattice angles, any free positional parameters of atoms within the unit cell that are allowed by the symmetry, the ADPs, and δ_1 or δ_2 (see Section 2.2 for a reminder on what these physically represent). For a given dataset it may be advantageous to deviate from this order. Nonetheless, this order is generally an excellent starting point.

2.2.3 Common challenges and pitfalls

As useful as the PDFgui is, it is not without its issues. Overcoming them requires a bit of problem solving and physical intuition for the material under analysis.

Unfortunately, it is not uncommon for fits to return physically impossible, or unlikely, values. For example, negative values of δ_1 or δ_2 would indicate peak broadening (see Section 2.1.1, Eq. (2)), which would in turn indicate that atomic motion is *less* correlated at smaller distances, than at larger distances. Ordinarily, the PDFgui will return negative values for δ_1 or δ_2 if you are using both as fitting parameters simultaneously. This is because they try to compensate for each other, leading one to be positive and way too big, and the other to be negative. The best way to correct this is to only use δ_1 or δ_2, but never both.

Another challenge is that fitting parameters plateau and cease improving, even though the fit is quantitatively, or qualitatively, poor. In more technical terms, this means that the fit error has reached a relative minimum, but not the global minimum and therefore there is still room for

further optimization. This plateau will occur if you provide suboptimal initial conditions and can easily be fixed by tweaking the initial conditions until the fit begins to improve again.

2.3 diffPy.mpdf Package

For mPDF analysis, I turn to an entirely separate piece of software. The diffPy.mpdf package [19] is a Python package containing tools for calculating the mPDF (see Section 2.1.2) from magnetic structures. By specifying a diffpy.structure object, propagation vectors, and basis vectors (see Section 2.1.2) the user can generate magnetic configurations and calculate the mPDF. Once the mPDF has been calculated, the user can then run a fit to the mPDF by refining the parameters described in Section 2.1.2.

2.3.1 Temperature Subtraction and Data Smoothing

Temperature subtraction and data smoothing are two methods that help remove unneeded information from the data in order to clarify the properties that *are* of interest. These methods are useful for isolating the mPDF signal, since it is typically much smaller than the atomic PDF signal. Physical justifications for these methods are included below.

The materials I analyzed exhibit ferromagnetic properties that are of interest [6,8]. Below their transition temperatures (see Section 1.2), ferromagnetic samples gain a stronger ferromagnetic signal. I can subtract a high-temperature data set showing no ferromagnetic signal from the low-temperature ferromagnetic signal without losing any information relevant to my investigation, with the added benefit of removing temperature-independent noise. This makes the ferromagnetic signal much more apparent and allows for a more accurate estimation of the material's magnetic properties.

Data smoothing can also be used to clean up the data. Essentially, data smoothing means I don't include some of the data when I inverse Fourier transform into real space. Because magnetic scattering only occurs up to about 8 $Å^{-1}$, all neutron diffraction data beyond this can be left out of the inverse Fourier transform without adversely impacting the magnetic signal; this is essentially a low-pass Fourier filter. I did this filtering by using diffPy's smoothData function. Filtering in this way removes high-frequency noise—that is often non-physical anyway—as well as other signals that, although possibly related to atomic structure, have nothing to do with the magnetic signal. The filter is applied as a convolution with the sinc function in real space, which is equivalent to a step-function cutoff in *Q*-space.

2.3.2 Common challenges and pitfalls

The fitting parameters described in Section 2.1.2 can sometimes refine to physically unacceptable values. For example, if the ordered scale factor refines to a negative value in a ferromagnet, then we should reject those values. This is because this value being negative would suggest the material does not have physically permissible magnetic correlations.

Another physically unacceptable case is that of a negative damping factor. A negative damping factor would indicate an increase in magnetic signal with distance, rather than a decrease, which contradicts some of the most basic laws of magnetostatics.

Fits can also be of suboptimal quality if the user specifies bad initial conditions. This can be fixed by experimenting with initial conditions until a fit is reached that is high quality and has all physically acceptable refinement parameters. I verified that the final fits were correct by checking that they fit the data at all the most prominent peaks and that no peaks were missed.

Chapter 3 Results and Conclusions

3.1 Li(Zn,Mn)As results and analysis

In this section, I will present the results of applying PDF and mPDF methods to neutron scattering data from Li(Zn,Mn)As. I will also analyze qualitative trends of these results in preparation for a discussion on the connections between the structural and magnetic properties of Li(Zn,Mn)As. I will analyze both the parent compound, LiZnAs, and the optimally doped compound, $Li_{1.1}Zn_{0.9}Mn_{0.1}As_{1.0}$. The parent compound is nonmagnetic and is purely semiconducting, while the doped compound shows metallic conductivity due to the presence of excess lithium and exhibits ferromagnetic behavior below 50 K.

3.1.1 Atomic PDF fit results

Figure 3.1 shows a PDF fit to x-ray diffraction data for the optimally doped compound. Note that all points are equally weighted when performing the fit, since the experimental uncertainty is uniform as a function of *r*. The error, or fit residual, is relatively small over the entire fitting range, with no regions of significantly higher error. Therefore, it would seem that the local and global structures are very similar. If the local structure had significant distortions or deviations from the longer-range structure, I would expect a much larger error at low r.

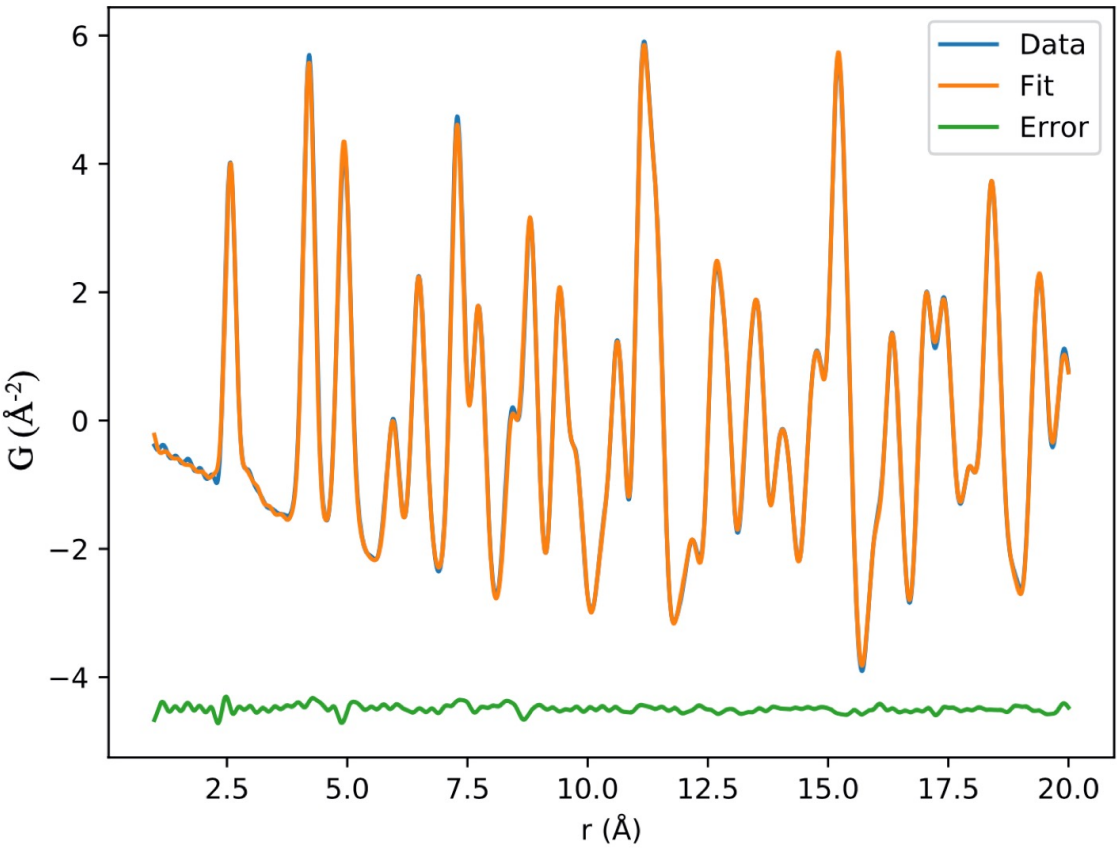

Figure 3.1 PDF fit for x-ray diffraction data from optimally doped Li(Zn,Mn)As. The blue line represents the collected data, the orange line the PDF fit, and the green line the difference between the data and the fit. The error has been offset by -4.5 for visual clarity.

Both Li(Zn,Mn)As compounds have a cubic structure, specifically antifluorite [20] (see Figure 3.2), so I only had one lattice constant to refine. Figure 3.3 and Figure 3.4 show the fitted values of the lattice parameter for data collected from neutron scattering for the parent compound and the optimally doped compound, respectively. The lattice parameter was calculated using PDFgui from 2 to 300 K. Both figures contain plots of PDF fits performed over short-, full-, and long-range data sets. Here, short range refers to fits from 1 to 6 Å, long range from 6 to 30 Å, and full range from 1 to 30 Å.

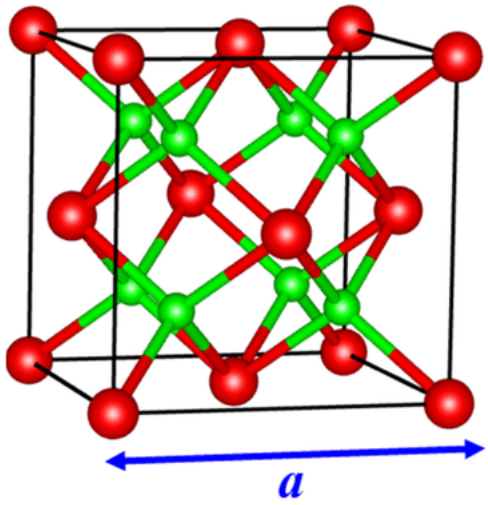

Figure 3.2 Example of an antifluorite lattice. Atomic positions are shown as red and green dots. Image from A. Annamareddy and J. Eapen, Entropy **19**, 227 (2017).

In each figure, there is qualitative agreement in trends of the fitted lattice parameter between short-, long-, and full-range fits. In each, there is such good agreement between the long- and full-range fits that only one is clearly distinguishable.

There is a slight offset between the short-range fits and the long- and full-range fits. This may suggest that there is some small local bond lengthening. However, this does not suggest that the local and global crystal families are different; rather, both are of the same crystal family, namely cubic, but with slightly different lattice parameters. Furthermore, there is an r-dependence that is introduced to the fitted lattice parameter when using PDF data processing. This data artifact, which is a result of slight asymmetries in the Bragg peaks when Fourier transformed, could also account for this offset. Therefore, whether this offset is due to actual bond lengthening or to a data artifact, the offset is not physically relevant to the current analysis.

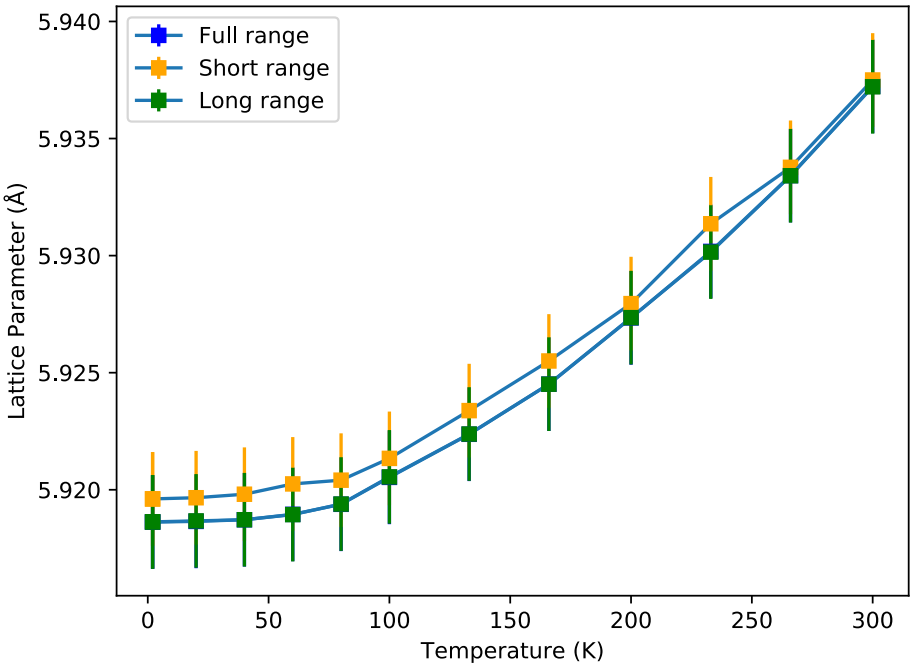

Figure 3.3 Fitted lattice parameter for the parent compound using short-, long-, and full-range data. The short-range fits (orange) were performed on data from 1 to 6 Å. The long-range fits (green) were performed on data from 6 to 30 Å. The full-range fits (blue) were performed on data from 1 to 30 Å.

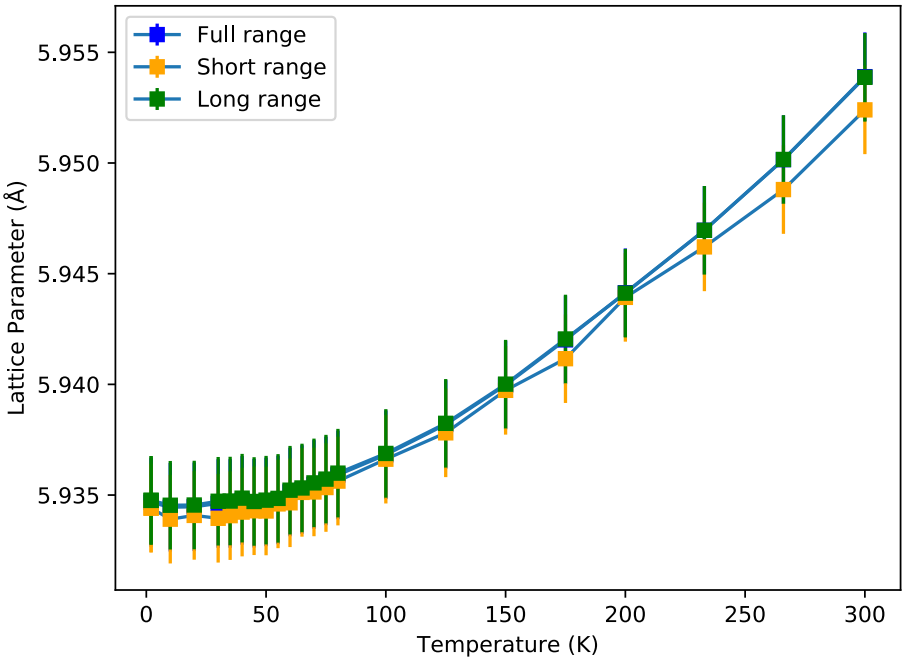

Figure 3.4 Fitted lattice parameter for optimally doped compound using short-, long-, and full-range data. The short-range fits (orange) were performed on data from 1 to 6 Å. The long-range fits (green) were performed on data from 6 to 30 Å. The full-range fits (blue) were performed on data from 1 to 30 Å.

The separation distances between pairs of manganese atoms were calculated using PDFgui's 'Calculate bond length' feature. These separation distances will be important for the discussion of magnetic correlations that follows in Section 3.1.2. These separation distances are tabulated in TABLE 1.

TABLE 1. Separation distances of manganese atoms in optimally doped Li(Zn,Mn)As compound from 1.5 to 10.0 Å. All distances were calculated at 2 K.

Separation (Å)
4.19(6)
5.93(4)
7.26(8)
8.39(2)
9.38(3)

3.1.2 Magnetic PDF fit results

Temperature subtraction of magnetic signals and data smoothing (see Section 2.3.1) were used in conjunction with mPDF analysis in order to reach accurate mPDF fits for the materials under investigation. Figure 3.5 represents the results of applying these methods to the optimally doped Li(Zn,Mn)As compound. The parent compound was not analyzed in this way because it lacks manganese, which is the magnetic dopant in the optimally doped compound.

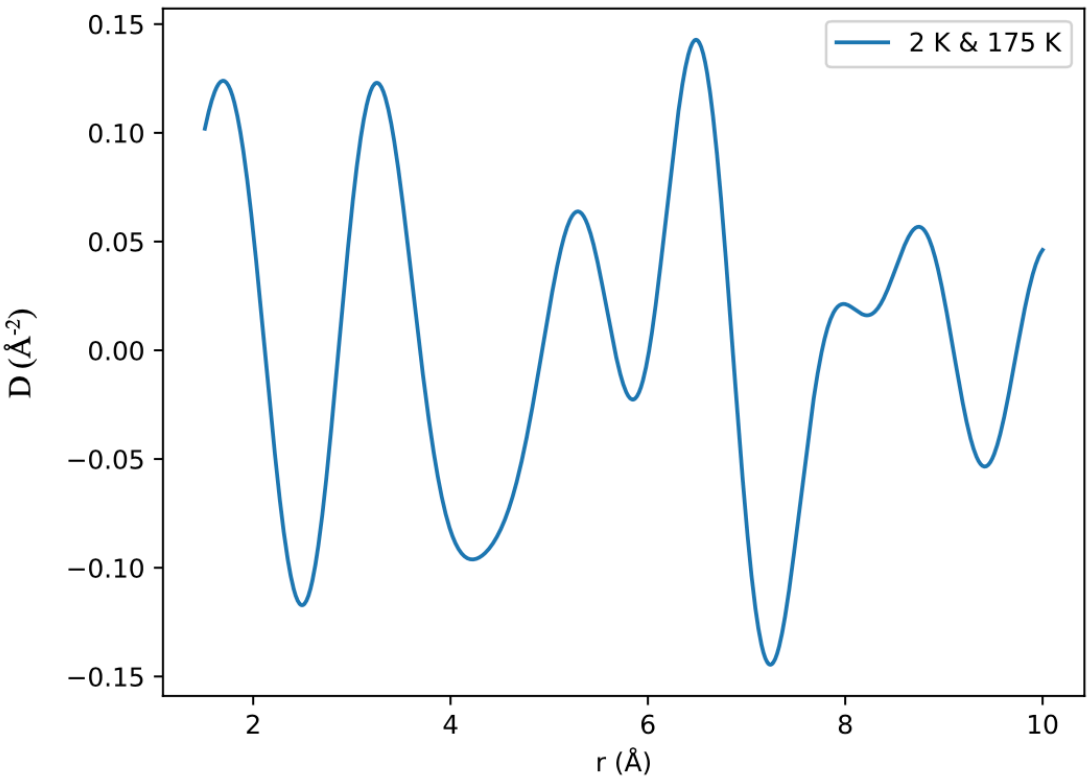

Figure 3.5 Smoothed temperature-subtraction mPDF data for optimally doped Li(Zn,Mn)As compound. Data collected at 175 K were subtracted from data collected at 2 K. Additionally, magnetic correlations only act up to 8 $Å^{-1}$ so the data were limited to this through smoothing.

The first peak in Figure 3.5 is an artifact from Fourier transforming high-frequency noise and does not encode any physically important information. Similarly, the following peak and trough do not represent actual physical moments. These claims are further supported by referencing the lattice parameter calculated for this material (see Figure 3.4) and the separation distances of manganese atom pairs (see TABLE 1)—manganese atoms are only found to be separated from each other by 4.196, 5.934, 7.268, 8.392, and 9.383 Å within the 10 Å window shown. Also, I expect positive peaks at these separation distances, as positive peaks would indicate ferromagnetic alignment. As it does not make physical sense that there be magnetic alignment at separation distances that don't correspond to that of manganese pairs, these first few peaks cannot possibly correspond to actual magnetic moments. At and beyond 4.0 Å, we see

positive peaks at locations that do not correspond to the separation distances of manganese pairs. Furthermore, there are *negative* peaks near the manganese separation distances, which could indicate antiferromagnetic alignment. However, it is known that this material is ferromagnetic [6], so these negative peaks are unlikely to represent the true mPDF. Therefore, the signal shown in Fig. 3.5, including both positive and negative peaks, is very unlikely be the true mPDF and is instead likely to be due to random noise or other artifacts in the data. This indicates the mPDF signal, if present, is smaller than the sensitivity of the experiment.

3.1.3 Analysis of Li(Zn,Mn)As results

The data presented in Section 3.1.1 suggest that Li(Zn,Mn)As does not have any significant differences in its local and average structures. This trend holds over all temperatures tested (2 K – 300 K). Therefore, both the optimally doped and parent compounds of Li(Zn,Mn)As have uniform crystal structure over all tested temperatures, including above and below the Curie temperature of 50 K.

As seen in Section 3.1.2, the optimally doped Li(Zn,Mn)As compound does not exhibit any peaks that correspond to the locations of manganese. Therefore, the compound does not have any magnetic correlations that were strong enough to be detected by my methods of analysis, which is to be expected due to this compound's weak ferromagnetism.

Therefore, the optimally doped compound of Li(Zn,Mn)As exhibits neither local structural distortions from the global structure nor any magnetic correlations between manganese spins that are observable within the sensitivity of the mPDF data.

3.2 $(Ba,K)(Zn,Mn)_2As_2$ results and analysis

In this section, I will present the results of applying PDF and mPDF methods to neutron scattering data from $(Ba,K)(Zn,Mn)_2As_2$. I will also analyze qualitative trends of these results in preparation for a discussion on the connections between the structural and magnetic properties of $(Ba,K)(Zn,Mn)_2As_2$. I will analyze both the parent compound, $BaZn_2As_2$, and the optimally doped compound, $Ba_{0.7}K_{0.3}(Zn_{0.85}Mn_{0.15})_2As_2$.

3.2.1 Atomic PDF fit results

Figure 3.6 shows a PDF fit to x-ray diffraction data collected for the optimally doped $(Ba,K)(Zn,Mn)_2As_2$. There is a noticeable increase in the magnitude of the error below 4 Å where there are obvious features in the data that the fit does not capture.

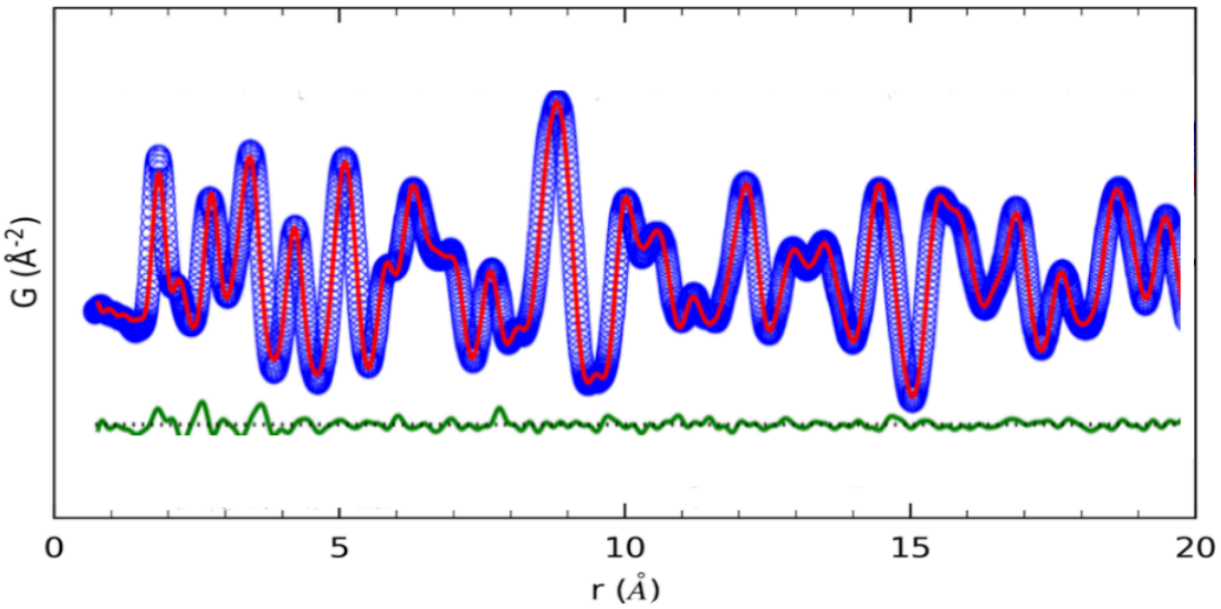

Figure 3.6 PDF fit for x-ray diffraction data from optimally doped $(Ba,K)(Zn,Mn)_2As_2$. The blue dots represent the collected data, the orange line the PDF fit, and the green line the difference between the data and the fit. The larger features in the fit residual at low r indicate local deviations from the long-range structure. The error has been vertically offset for visual clarity. The size of the data points is not physically significant.

To further investigate the structure at low r, I turn to the refinements for the lattice constants. Both $(Ba,K)(Zn,Mn)_2As_2$ compounds have tetragonal structure [8], so I have two lattice constants to refine. Figure 3.7 shows an arbitrary body-centered tetragonal unit cell for reference.

Figure 3.8 and Figure 3.9 show the fitted values of lattice constants a and c, respectively, for neutron scattering data. Short-range fits were performed on data from 0.5 to 6 Å and full-range fits were performed from 0.5 to 20 Å. Both figures exhibit clear differences in the qualitative trends of the lattice parameter when fitted over short-range and full-range data. These trends, combined with the greater error below 4 Å, all seem to indicate that there are local structural distortions from the global structure in the optimally doped $(Ba,K)(Zn,Mn)_2As_2$ compound.

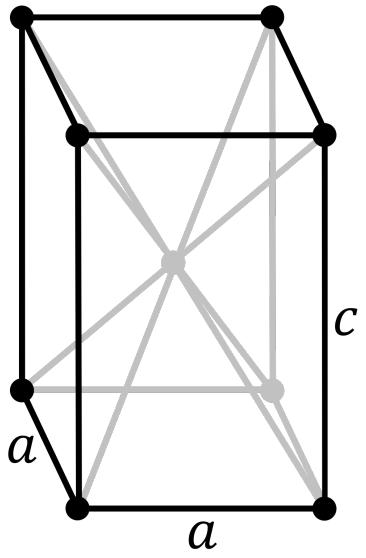

Figure 3.7 A body-centered tetragonal unit cell. Each black dot represents an atomic site. The sides labeled a are of the same length, while c is of a different length. All sides meet at right angles.

Since manganese is the only magnetic atom in this compound, it will be important for the magnetic analysis in Section 3.2.2. The separation distances of manganese pairs were calculated using PDFgui's 'Calculate bond length' feature and are shown in TABLE 2.

TABLE 2. Separation distances of manganese atoms in optimally doped $(Ba,K)(Zn,Mn)_2As_2$ compound from 1.5 to 10.0 Å. All distances were calculated at 2 K.

Position (Å)
2.90(9)
4.114)
5.81(9)
6.50(5)
6.71(8)
7.32(1)
7.87(8)
8.22(9)
8.72(8)
8.88(8)
9.20(0)
9.35(2)

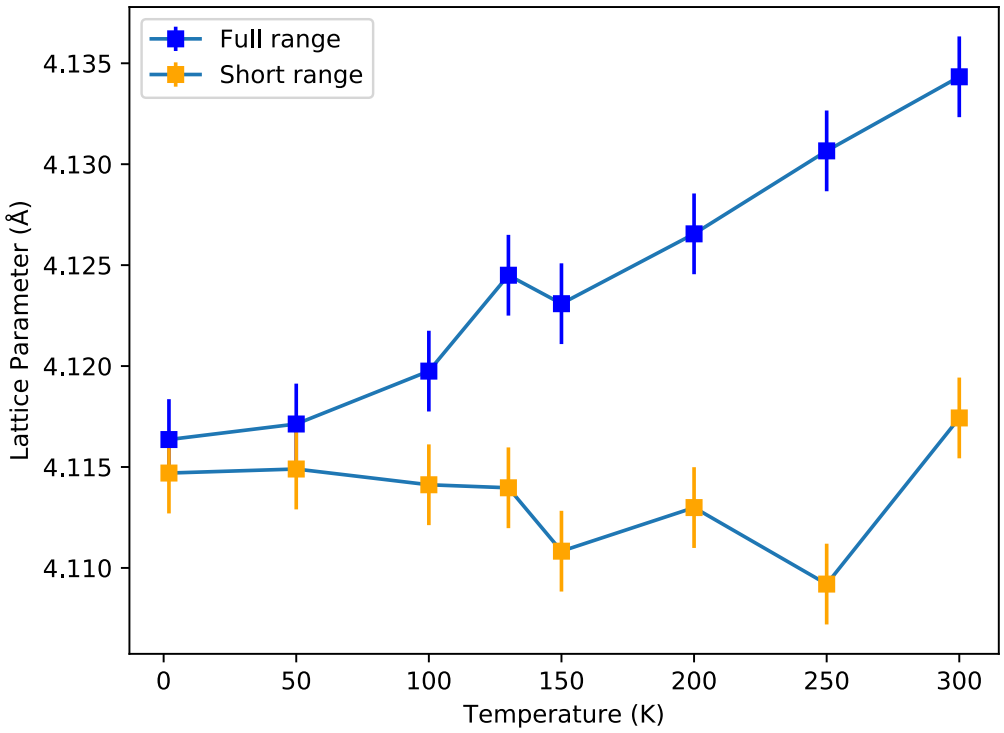

Figure 3.8 Short- and full-range fitted value of lattice parameter *a* from 2 to 300 K.

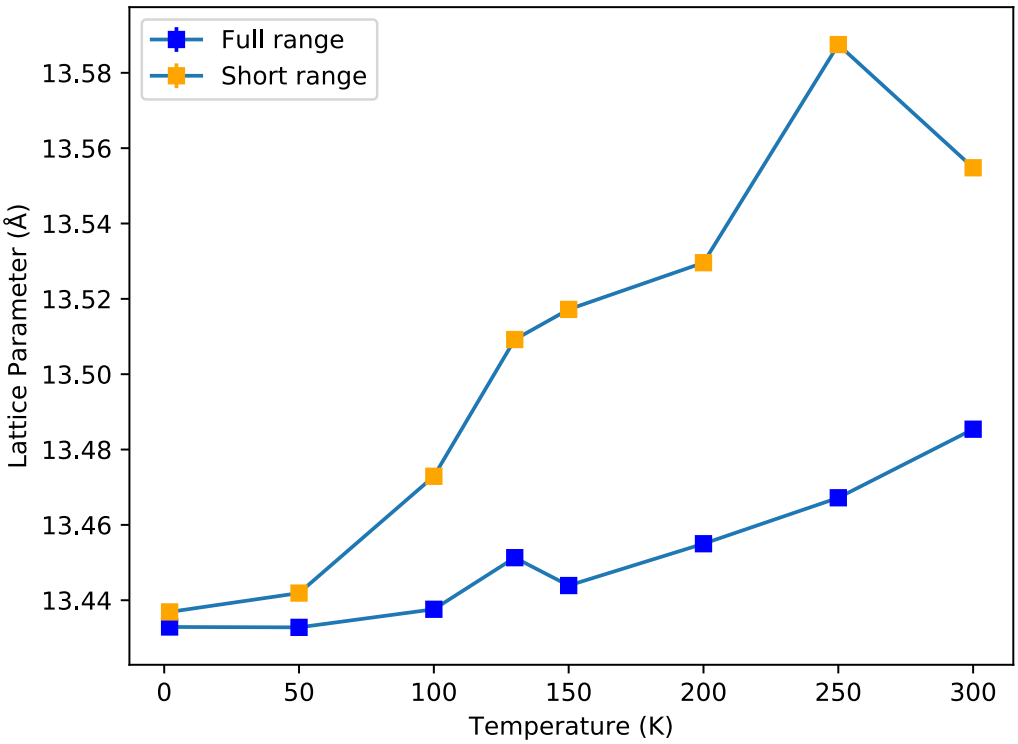

Figure 3.9 Short- and full-range fitted value of lattice parameter *c* from 2 to 300 K.

3.2.2 Magnetic PDF fit results

mPDF fits were performed on neutron scattering data collected for the optimally doped $(Ba,K)(Zn,Mn)_2As_2$ compound. Both an antiferromagnetic model and a ferromagnetic model were used to separately fit the data.

Figure 3.10 shows the results of fitting an antiferromagnetic model to neutron scattering data for the optimally doped $(Ba,K)(Zn,Mn)_2As_2$ compound. The fit is of very poor quality over the entire range. While the fit does seem to somewhat follow the data's trends below 5 Å, overall the fit does not reflect the significant features in the data. This indicates that the material is likely not antiferromagnetic, a result that is to be expected, since it is supposed to be a ferromagnet [8].

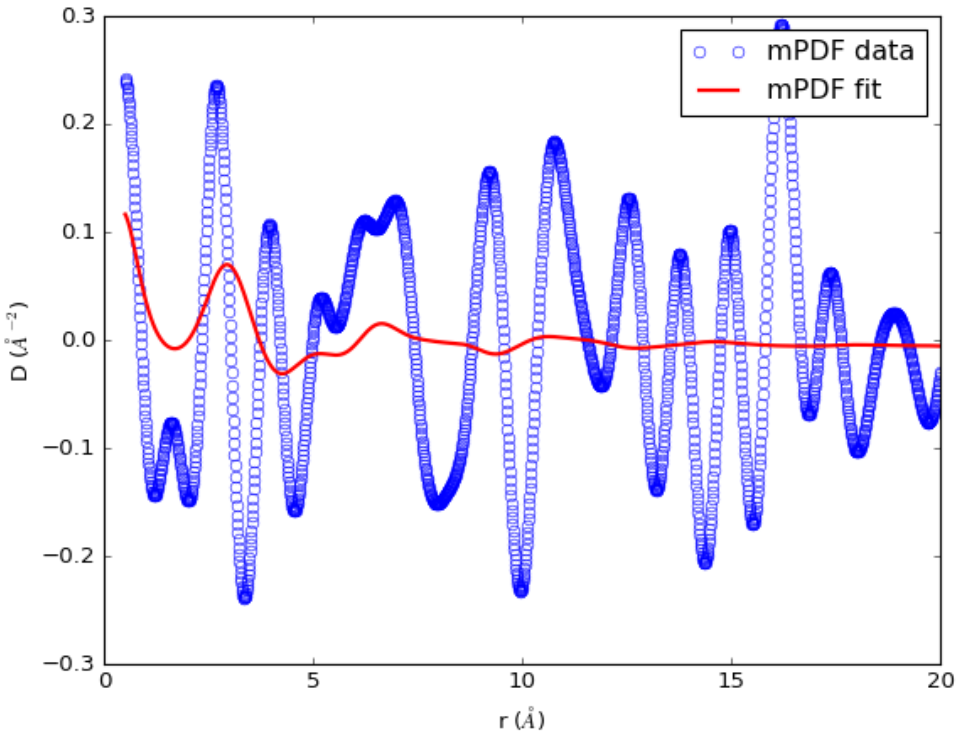

Figure 3.10 mPDF antiferromagnetic fit to neutron scattering data from optimally doped $(Ba,K)(Zn,Mn)_2As_2$.

Figure 3.11 shows the results of fitting a ferromagnetic model to the data, with a magnetic basis vector of (0, 0, 1). Fits were performed using other magnetic basis vectors; however, all of said fits had a higher error and less qualitative agreement with the data. Those fits were not included here because of their low quality. Although the quality of the fit is not of extremely high quality, the trends in the data are somewhat captured by the fit. Since the mPDF is more than an order of magnitude smaller than the atomic PDF, it is not surprising that the fit quality is only marginal. These results provide good evidence that there are indeed important magnetic correlations in this material, and further confirms that the material is in fact ferromagnetic. Discrepancies between the data and fit could likely be mitigated by further refining the magnetic propagation vector, as well as other properties of the magnetic structure.

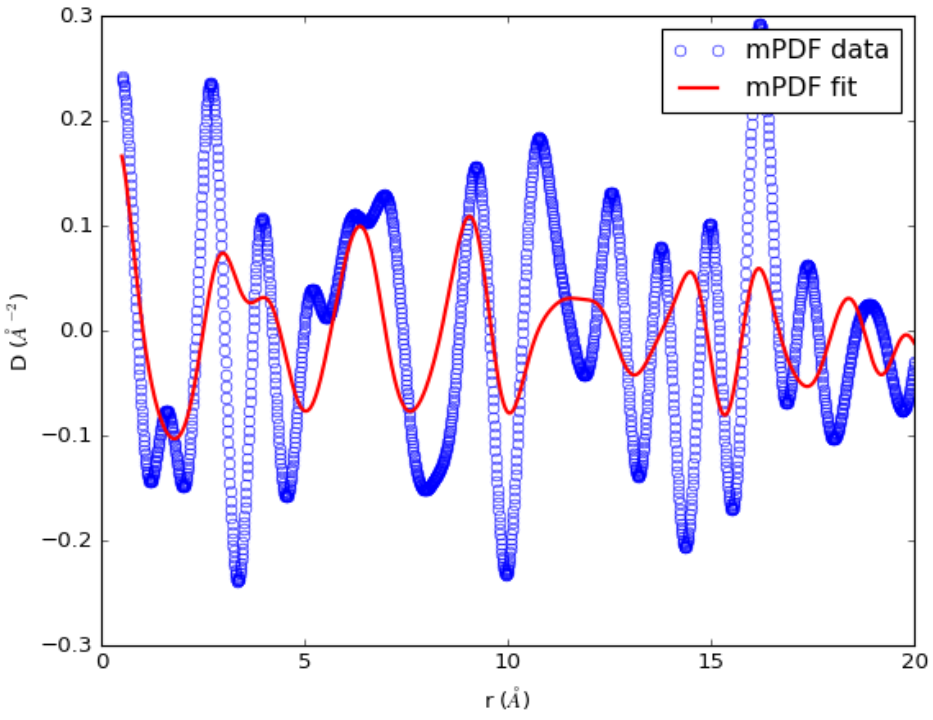

Figure 3.11 mPDF ferromagnetic fit to neutron scattering data from optimally doped $(Ba,K)(Zn,Mn)_2As_2$.

For the purpose of this research it is sufficient to note that the magnetic model somewhat fits. A high-quality fit is not necessary to demonstrate the short-range magnetic order that is of interest. In particular, below 10 Å there are a number of peaks which indicate magnetic moment correlation over short-range. Additionally, there are prominent positive peaks at the separation distances of manganese atoms (see TABLE 2) which further indicates some kind of magnetic correlations.

3.2.3 Analysis of $(Ba,K)(Zn,Mn)_2As_2$ results

The optimally doped compound exhibits increased error below 4 Å. Additionally, the error in this range seems to exhibit distinct structure. Short-range fits demonstrate that indeed there is a difference between the local and average structures. Furthermore, in spite of their poor overall qualitative agreement with the data, the ferromagnetic mPDF fit *does* capture some of the data's most important features and indicate that there is important ferromagnetic structure and short-range magnetic order.

3.3 Comparison of Li(Zn,Mn)As and $(Ba,K)(Zn,Mn)_2As_2$

The optimally doped Li(Zn,Mn)As compound was determined to have no meaningful differences between its local and average structure. Also, it was found to lack any significant magnetic order observable within the experimental sensitivity.

The opposite was found to be true on both accounts for the optimally doped $(Ba,K)(Zn,Mn)_2As_2$ compound. It has nonnegligible local differences from its average structure and observable magnetic correlations in the mPDF data, indicating significantly stronger ferromagnetism.

Therefore, there is an apparent connection between local structural distortions and short-range magnetic order in these two dilute magnetic semiconductors. It could be mere coincidence that the system with stronger ferromagnetism has significant local structural deviations while the weaker magnetic system has no such deviations, yet there may also be a sensible physical justification for this. Specifically, the details of the local arrangement of atoms determines the strength of the magnetic exchange interactions that mediate the ferromagnetism. The local distortions in the $(Ba,K)(Zn,Mn)_2As_2$ compound may result in stronger magnetic interactions and therefore more robust ferromagnetism. Verifying this hypothesis is beyond the scope of the present study.

3.4 Future work

Having observed a connection between magnetic correlations and local atomic structure in these two materials, the most natural extension of this research will be to investigate whether or not these connections are true of dilute magnetic semiconductors in general. By way of said investigation, our understanding of dilute magnetic semiconductors will improve and expand so that they may be applied to spintronics, quantum computing, and other technologies.

In addition to investigating other materials, it would also be beneficial to perform density functional theory (DFT) calculations on the magnetic properties of Li(Zn,Mn)As and $(Ba,K)(Zn,Mn)_2As_2$. Specifically, the formation enthalpy and magnetic exchange interactions should be calculated for structures both with and without local structural distortions. This would allow for a more thorough confirmation of the results I presented.

3.5 Summary and conclusion

The results heretofore presented serve to further improve our understanding of Li(Zn,Mn)As and (Ba,K)$(Zn,Mn)_2As_2$, as well as verify existing literature on them [6,8]. These results pave the way for further investigation of related dilute magnetic semiconductors. This will allow for a greater understanding of dilute magnetic semiconductors in general, which in turn will allow for the advancement of science and technology in many ways, both foreseen, such as spintronics and quantum computing, and unforeseen. But for now, it would seem that when searching for dilute magnetic semiconductors with strong ferromagnetism, one would do well to consider those with local structural distortions.

Index

Bibliography

[1] S.R. Khetani and S.N. Bhatia, "Microscale culture of human liver cells for drug development", Nature Biotechnology **26**, 120 (2007).

[2] M.R. Hoffmann, S.T. Martin, W. Choi, and D.W. Bahnemann, "Environmental Applications of Semiconductor Photocatalysis", Chemical Reviews **95**, 69 (1995).

[3] https://thinkcomputers.org/the-history-of-the-hard-drive/, accessed January 2020.

[4] T. Dietl and H. Ohno, "Dilute ferromagnetic semiconductors: Physics and spintronic structures", Reviews of Modern Physics **86**, 187 (2014).

[5] Y. Li, J. Li, Z. Yu, W. Li, M. Zhu, H. Jin, Y. Liu, Y. Li, and K. Skotnicova, "Study on the high magnetic field processed ZnO based diluted magnetic semiconductors", Ceramics International **45**, 19583 (2019).

[6] Z. Deng, C. Jin, Q. Liu, X. Wang, J. Zhu, S. Feng, L. Chen, R. Yu, C. Arguello, T. Goko, F. Ning, J. Zhang, Y. Wang, A. Aczel, T. Munsie, T. Williams, G. Luke, T. Kakeshita, S. Uchida, W. Higemoto, T. Ito, B. Gu, S. Maekawa, G. Morris, and Y. Uemura, "Li(Zn,Mn)As as a new generation ferromagnet based on a I-II-V semiconductor", Nature Communications **2**, (2011).

[7] K. Zhao, Z. Deng, X.C. Wang, W. Han, J.L. Zhu, X. Li, Q.Q. Liu, R.C. Yu, T. Goko, B. Frandsen, L. Liu, F. Ning, Y.J. Uemura, H. Dabkowska, G.M. Luke, H. Luetkens, E. Morenzoni, S.R. Dunsiger, A. Senyshyn, P. Böni, and C.Q. Jin, "New diluted magnetic semiconductor with Curie temperature up to 180 K and isostructural to the '122' iron-based superconductors", Nature Communications **4**, (2013).

[8] B.A. Frandsen, Z.W. Gong, M.J. Terban, S.J.L. Banerjee, B. Chen, C. Jin, M. Feygenson, Y. Uemura, and S. Billinge, "Local atomic and magnetic structure of dilute magnetic semiconductor (Ba,K)(Zn,Mn)$_2$As$_2$", Physical Review B **94**, (2016).

[9] J.G. Kirkwood, "Statistical mechanics of fluid mixtures", The Journal of Chemical Physics **3**, 300 (1935).

[10] T. Proffen, S.J.L. Billinge, T. Egami, and D. Louca, "Structural analysis of complex materials using the atomic pair distribution function – a practical guide", Zeitschrift Für Kristallographie - Crystalline Materials **218**, (2003).

[11] H. Zheng, L. Zhu, S. Jiang, Y. Wang, S. Liu, S. Lan, and F. Chen, "Role of Ni and Co in tailoring magnetic and mechanical properties of $Fe_{84}Si_2B_{13}P_1$ metallic glass", Journal of Alloys and Compounds **816**, 152549 (2020).

[12] T. Egami and S.J.L. Billinge, *Underneath the Bragg Peaks: Structural Analysis of Complex Materials* (Elsevier, Amsterdam, 2012).

[13] https://en.wikipedia.org/wiki/Pair_distribution_function, accessed February 2020.

[14] T. Proffen and S.J.L. Billinge, "*PDFFIT*, a program for full profile structural refinement of the pair distribution function", Journal of Applied Crystallography **32**, 572 (1999).

[15] https://www.diffpy.org/products/pdfgui.html, accessed February 2020.

[16] B.A. Frandsen, X. Yang, and S.J.L. Billinge, "Magnetic pair distribution function analysis of local magnetic correlations", Acta Crystallographica Section A Foundations and Advances **70**, 3 (2013).

[17] https://en.wikipedia.org/wiki/Neutron, accessed February 2020.

[18] B.A. Frandsen and S.J.L. Billinge, "Magnetic structure determination from the magnetic pair distribution function (mPDF): ground state of MnO", Acta Crystallographica Section A Foundations and Advances **71**, 325 (2015).

[19] https://www.diffpy.org/products/mPDF.html, accessed February 2020.

[20] K. Kuriyama and F. Nakamura, "Electrical transport properties and crystal structure of LiZnAs", Physical Review B **36**, 4439 (1987).